PAPER

NJC
www.rsc.org/njc

Heterocyclic quinol-type fluorophores.† Synthesis of novel imidazoanthraquinol derivatives and their photophysical properties in benzene and in the crystalline state‡

Yousuke Ooyama, Takato Nakamura and Katsuhira Yoshida*

Department of Material Science, Faculty of Science, Kochi University, Akebono-cho, Kochi 780-8520 Japan. E-mail: kyoshida@cc.kochi-u.ac.jp; Fax: +81 88-844-8359

Received (in Durham, UK) 6th July 2004, Accepted 10th November 2004
First published as an Advance Article on the web 4th January 2005

An isomeric pair of novel imidazoanthraquinol fluorophores **2** and **3** exhibiting two tautomeric forms (**A** and **B**) that are possible for the imidazole ring have been developed. In order to control the tautomeric form to improve the fluorescence properties, the *N*-butylated imidazole derivatives **6** and **7** have further been synthesized. The fluorescence intensity of the quinols was in the order **3** ≪ **6** < **7** < **2** in benzene, which is quite different from the order **3** ≪ **2** ≪ **6** < **7** in the crystalline state. To investigate the effect of *N*-alkylation of imidazole ring on the photophysical properties of the quinol fluorophores in solution and in the crystalline state, we have performed semi-empirical molecular orbital calculations (AM1 and INDO/S) and X-ray crystallographic analysis. On the basis of the results of calculations and the X-ray crystal structures, the *N*-alkylation effects on the chemical structure of the quinol fluorophores and on their solid-state photophysical properties are discussed.

Introduction

Organic fluorophores have received much attention in recent years, because of their many applications in the optoelectronics industry such as dye lasers, solar energy converting materials, and emitters in optoelectronic devices.[1] A great number of fluorescent compounds have been developed and the relationship between their chemical structure and fluorescence properties examined. However, very little is known about the influence of molecular packing structure of fluorophores on their solid-state fluorescence properties.[2–6] Therefore, the number of fluorescent compounds that exhibit strong solid-state emission properties is relatively limited.

In Part 1 and Part 2 of this series of the heterocyclic quinol-type fluorophores, we have reported benzofuranonaphthoquinol-type fluorophores that can form crystalline inclusion compounds with various amine molecules.[4] The fluorescence of the quinols in the solid state is greatly quenched in comparison with that in solution. However, the fluorescence of the quinol crystals is enhanced in various degrees depending on the enclathrated amine molecules. These specific properties of the quinol fluorophores that exhibit dramatic fluorescence enhancement upon complexation with guest molecules will be useful for fundamental research into solid state fluorescence and for the development of new intense solid-emissive materials. In connection with above research, we have developed novel imidazoanthraquinol fluorophores **2** and **3** in which two tautomeric forms (**A** and **B**) are possible for the imidazole ring.[7,8] On account of the tautomerism of the imidazole ring, the two isomeric fluorophores were considered to show a variety of photophysical properties in solution and in the crystalline state. Moreover, new compounds exhibiting intense solid-fluorescence properties were expected to be obtained by control of the tautomeric form by *N*-alkylation of the imidazole ring. Therefore, we have further synthesized the *N*-butylated derivatives **6** and **7**. To elucidate the relationship between the photophysical properties and the chemical and crystal structures, semi-empirical molecular orbital calculations (AM1 and INDO/S) and the X-ray crystallographic analysis of **2a**, **3a**, **6** and **7** have been carried out.

Results and discussion

Synthesis of imidazoanthraquinol fluorophores

The synthesis of the isomeric pairs of imidazoanthraquinol fluorophores is outlined in Scheme 1. We first prepared the starting heterocyclic quinone **1** by refluxing an equimolar amount of 1,2-diaminoanthraquinone with *p*-(diethylamino)-benzaldehyde in acetic acid in the presence of copper(II) acetate. Next, the heterocyclic quinone-type dye **1** was allowed to react with organometallic reagents to give the isomeric pairs of quinol compounds **2** and **3** in which two tautomeric forms (A and B) are possible for the imidazole ring. As shown in Table 1, the ratios of the products (**2**:**3**) were greatly dependent on steric factors of the organometallic reagents. For example, the reaction with MeMgI afforded a **2a**:**3a** ratio of 31:69 (entry 1), whereas the reaction with MeLi afforded a **2a**:**3a** ratio of 83:17 (entry 2): the selectively of **2a** to **3a** being quite reversed. These results suggest that the relatively small MeLi could preferentially attack the more electrophilic carbonyl carbon to give **2a**, while the relatively large and heavily solvated MeMgI reagent attacks the less-hindered carbonyl carbon to give **3a**. The results given for entries 2–4 in Table 1 also suggest that the preparation of isomer **2** becomes difficult as the counteranion (R^-) of organo-lithium reagents becomes bulky. On the other hand, the synthesis of *N*-alkylated imidazoanthraquinol derivatives was achieved according to Scheme 2. The reaction of 1,2-diaminoanthraquinone with 1-iodobutane produced 1-amino-2-butylaminoanthraquinone **4** in 66% yield. The quinone **5** was synthesized in 77% yield by refluxing an equimolar amount of 1-amino-2-butylaminoanthraquinone

† Part 3. For Part 2, see: ref. 4b.
‡ Electronic supplementary information (ESI) available: Table S1 Crystal data and structure refinement parameter for the quinol derivatives **2a**, **3a**, **6** and **7**. See http://www.rsc.org/suppdata/nj/b4/b410311d/

DOI: 10.1039/b410311d

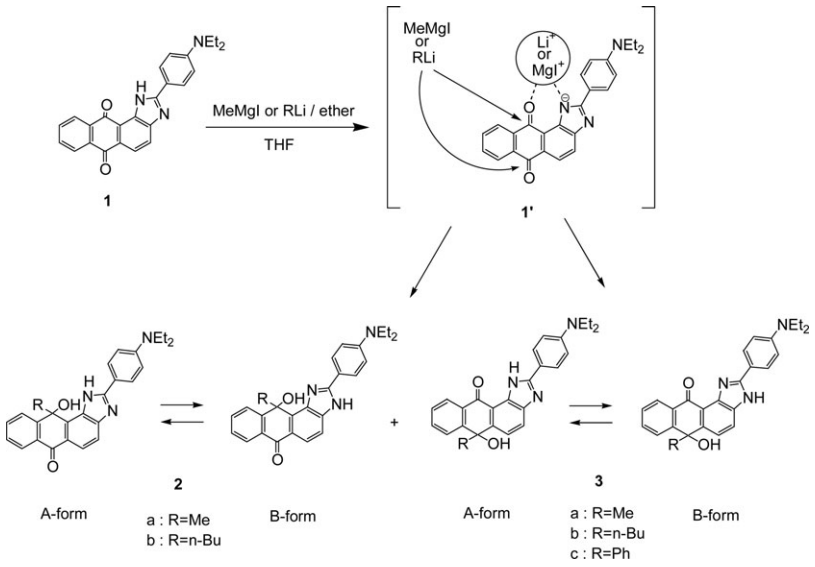

Scheme 1

Table 1 Synthesis of the quinols **2** and **3** by the reaction of **1** with organo-lithium or magnesium reagent

		Product			
Entry	Reagent	Quinols	Yield (%)	Ratio **2**:**3**	Recovery (%) of **1**
1	MeMgI	**2a** + **3a**	82.1	31:69	11.8
2	MeLi	**2a** + **3a**	66.5	83:17	17.0
3	*n*-BuLi	**2b** + **3b**	73.6	34:66	7.6
4	PhLi	**3c**	33.3	0:100	63.8

with *p*-(diethylamino)benzaldehyde in acetic acid in the presence of copper(II) acetate, and then the reaction of **5** with organometallic reagents at low temperature gave quinols **6** and **7** in 30 and 43% yields, respectively.

Spectroscopic properties of the imidazoanthraquinol fluorophores in solution

The absorption and fluorescence spectra of the quinol derivatives **2**, **3**, **6** and **7** in benzene are summarized in Fig. 1 and Table 2. The fluorescence spectra of the quinols were recorded at the wavelengths of the longest absorption maximum. The two kinds of isomers (**2**, **3** and **6**, **7**) have respectively the same donor–acceptor chromogens, but a marked difference in degree of the donor–acceptor conjugation, which leads to quite different absorption and fluorescence spectra in benzene.

The quinol **2a** exhibited absorption maximum at around 369 nm and structureless absorption band at around 316 nm and fluorescence band at around 469 nm ($\Phi = 0.20$). On the other hand, the compound **3a** exhibited two distinct absorption bands in the visible region at around 416 nm and 327 nm and the corresponding fluorescence band observed at around 480 nm; however, it was difficult to determine exactly its quantum yield because of a feeble fluorescence intensity. Comparing the absorption and fluorescence spectra of **2a** and **3a**, the quinol **2a** exhibits much stronger absorption and fluorescence intensities than the quinol **3a** in benzene. Because of the non-conjugated linkage of the substituents (R = Me, Bu and Ph) to the chromophore skeleton, the absorption and fluorescence spectra of the compounds belonging to the same type of isomers resemble each other very well.

In contrast, the *N*-butylated compounds **6** and **7** showed quite different absorption and fluorescence spectra compared to those of **2a** and **3a**. The absorption maxima of **6** ($\lambda_{max} = 352$ and 315 nm) and **7** ($\lambda_{max} = 389$ and 297 nm) were shifted to shorter wavelengths compared to those of **2a** and **3a**. The *N*-butylation of **2a** and **3a** adversely affected their fluorescence properties: the fluorescence quantum yield of **6** ($\lambda_{em} = 432$ nm, $\Phi = 0.028$) is smaller than that of **2a**, while the fluorescence

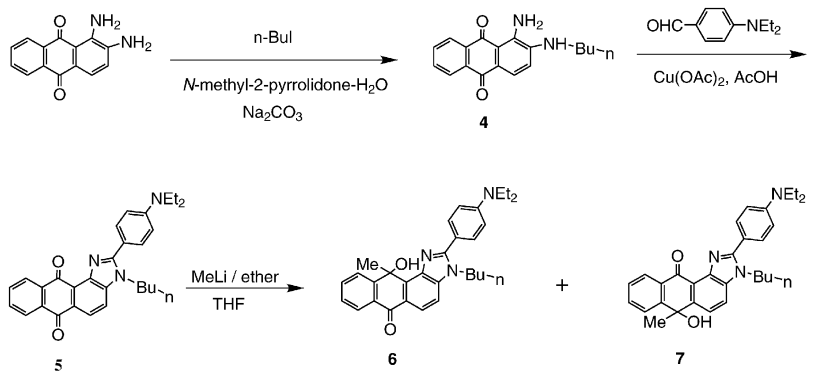

Scheme 2

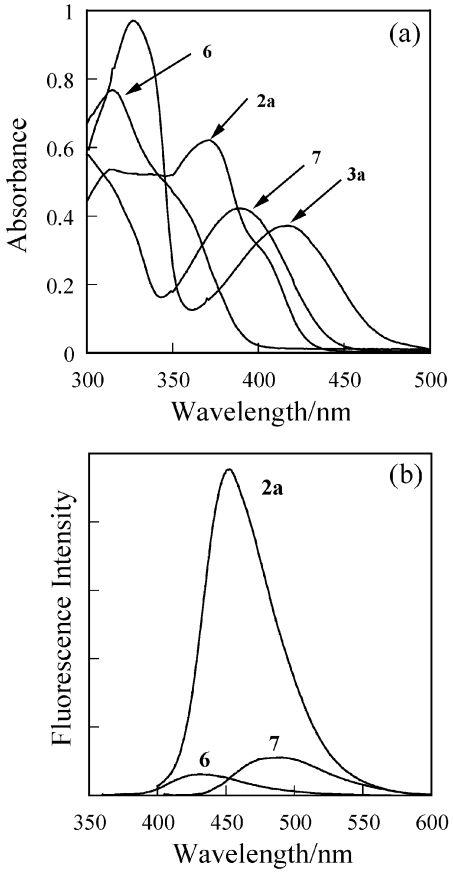

Fig. 1 (a) Absorption and (b) fluorescence spectra of compounds **2a**, **3a**, **6** and **7** in benzene.

quantum yield of **7** (λ_{em} = 497 nm, Φ = 0.041) is much larger than that of **3a**. These results show that the fluorescence quantum yield becomes smaller when the control of the tautomerism by the *N*-butylation decreases the degree of donor–acceptor conjugation as in the case of **6**, but when the control of the tautomerism increases the degree of donor–acceptor conjugation, as in the case of **7**, the fluorescence quantum yield becomes larger.

Semi-empirical MO calculations (AM1, INDO/S)

We have carried out semi-empirical molecular orbital (MO) calculations for the quinol fluorophores **2a** and **3a** (for both in A- and B-form), **6** and **7** by the INDO/S[9] after geometrical optimizations using MOPAC/AM1 calculations.[10] The calculated absorption wavelengths and the transition character of the first and second absorption bands are collected in Table 3.

The calculated torsion angles between the *p*-diethylaminophenyl group and the imidazole ring of the **2a** and **3a** are *ca.* 25–29° in spite of the tautomeric forms. On the other hand, the calculated torsion angles of **6** and **7** were *ca.* 55.4° and 49.1°, respectively, which is attributed to steric hindrance between the *N*-butyl group and the *p*-diethylaminophenyl group. The INDO/S calculations show that the oscillator strength (*f*) of the first excitation band (λ_{max} = 341 nm, *f* = 0.97) is larger than that of the second excitation band (λ_{max} = 314 nm, *f* = 0.21) in the case of **2a** in A-form, while in B-form the *f*-value of the second excitation band (λ_{max} = 309 nm, *f* = 0.63) is larger than that of the first excitation band (λ_{max} = 334 nm, *f* = 0.59). On the contrary, the *f*-value of the second excitation bands (λ_{max} = 306 nm, *f* = 0.69) is larger than that of the first excitation band (λ_{max} = 358 nm, *f* = 0.45) in the case of **3a** in A-form, while in the B-form the *f*-value of the first excitation band (λ_{max} = 352 nm, *f* = 0.67) is larger than that of the second excitation band (λ_{max} = 302 nm, *f* = 0.40). From the calculation data it was presumed that both of the compounds **2a** and **3a** probably exist in A-form in benzene. In respect of the donor–acceptor conjugation, the A-form of **2a** is more conjugative but the A-form of **3a** is less conjugative in comparison with the B-form of **3a**. In contrast, in the case of **6**, the *f*-value of first excitation band (λ_{max} = 324 nm, *f* = 0.21) is smaller than that of the second excitation band (λ_{max} = 294 nm, *f* = 0.76). In the case of **7**, the *f*-value of the first excitation band (λ_{max} = 343 nm, *f* = 0.48) is larger than that of the second excitation band (λ_{max} = 302 nm, *f* = 0.29). The wavelengths of the first and second excitation bands of **6** and **7** are shorter than those of **2a** and **3a**. These calculated absorption wavelengths and the oscillator strength values match relatively well the observed spectra in benzene, although the calculated absorption spectra are blue shifted. This deviation of the INDO/S calculations, giving high transition energies compared with the experimental values, has been generally observed.[11,12] The calculations also show that the first excitation bands for the four quinols are mainly assigned to the transition from the HOMO to the LUMO, where HOMO were mostly localized on the *p*-diethylaminophenyl and benzo-imidazole moieties, and the LUMO were mostly localized on the anthraquinol moiety. The calculated electron density changes accompanying the first electron excitation are shown in Fig. 2, which shows a strong migration of intramolecular charge-transfer character of the four quinols. As clearly seen, the calculated electron density changes of **6** and **7** are quite similar to those of the B-form of **2a** and **3a**, respectively. On the other hand, as shown in Fig. 3, the values of the dipole moment of the quinols are large except for that of the A-form of **3a**. It is noteworthy that the directions of the dipole moment differ between the A-form and the B-form in both **2a** and **3a**. In addition, the directions of the dipole moment of **6** and **7** are almost the same as those of the B-forms of **2a** and **3a**, respectively. These results clearly show that the *N*-alkylation of the imidazole ring of **2a** and **3a** can fix the tautomeric form and the resulting compounds **6** and **7** have the electronic natures corresponding to the B-forms of **2a** and **3a**, respectively.

Table 2 Absorption and fluorescence spectral data of **2**, **3**, **6** and **7** in benzene

Quinol	Absorption (Obs.) λ_{max}/nm (ε_{max}/dm^3 mol^{-1} cm^{-1})	Fluorescence (Obs.) λ_{em}/nm	Φ	SS[a] $\Delta\lambda_{max}$/nm
2a	369 (25 300), 316 (22 800)	469	0.20	100
2b	368 (26 200), 318 (22 700)	468	0.19	100
3a	416 (13 000), 327 (32 900)	480	<0.001	64
3b	415 (15 000), 327 (33 400)	468	<0.001	53
3c	420 (13 000), 328 (31 400)	—[b]	—[b]	—[b]
6	352 (18 000), 315 (32 300)	432	0.028	80
7	389 (17 700), 297 (24 500)	497	0.041	108

[a] Stokes shift value. [b] Too weak to be measured.

Table 3 Geometry optimization and calculated absorption spectra for the compounds **2a** and **3a** (for both in A- and B-form), **6** and **7**

Quinol	Torsion angle/° [a]	Absorption (calc.) λ_{max}/nm	f [b]	CI component [c]	μ/D [d]
2a-A-form	28.5	341	0.97	HOMO → LUMO (65%)	9.12
		314	0.21	HOMO → 1-LUMO (52%)	
2a-B-form	27.5	334	0.59	HOMO → LUMO (46%)	9.04
				HOMO → LUMO + 1 (22%)	
		309	0.63	HOMO → LUMO + 1 (63%)	
3a-A-form	27.8	358	0.45	HOMO → LUMO (65%)	3.04
		306	0.69	HOMO → LUMO + 1 (77%)	
3a-B-form	25.6	352	0.67	HOMO → LUMO (75%)	8.14
		302	0.40	HOMO → 1-LUMO (47%)	
				HOMO → LUMO + 1 (21%)	
6	55.4	324	0.21	HOMO → LUMO (41%)	9.82
				HOMO → 1-LUMO (18%)	
		294	0.76	HOMO → LUMO + 1 (73%)	
7	49.1	343	0.48	HOMO → LUMO (60%)	6.82
		302	0.29	HOMO → 1-LUMO (30%)	
				HOMO → 2-LUMO (27%)	

[a] Torsion angle between imidazole ring and *p*-diethylaminophenyl group. [b] Oscillator strength. [c] The transition is shown by an arrow from one orbital to another, followed by its percentage CI (configuration interaction) component. [d] The values of the dipole moment in the ground state.

Spectroscopic properties of the imidazoanthraquinol fluorophores in solid state

Interesting results have been obtained from the solid-state fluorescence excitation and emission spectra of the crystals **2a**, **3a**, **6** and **7**, which are shown in Fig. 4. The quinols **6** and **7** exhibit much stronger fluorescence intensities than **2a** and **3a**, the fluorescence intensity increases in the order **3a** ≪ **2a** ≪ **6** < **7** in the crystalline state, which is quite different from the order **3a** ≪ **6** < **7** < **2a** in benzene. The longest wavelength of fluorescence excitation and emission maxima of **2a** is located at around 520 and 567 nm, which are red-shifted by 151 and 98 nm in comparison with the values of the absorption and fluorescence maxima of **2a** in benzene, respectively. Such large bathochromic shifts of the absorption and fluorescence wavelengths on going from solution to the solid state have been observed in other chromophores having intramolecular charge transfer character.[13–15] The fluorescence excitation and emission maxima of **6** (λ_{ex} = 413 nm, λ_{em} = 457 nm) and **7** (λ_{ex} = 445 nm, λ_{em} = 513 nm) show a blue shift with intense fluorescence compared with those of **2a** and **3a**, respectively. While the fluorescence quantum yield of **2a** is *ca.* 7-fold larger than that of **6** in benzene, the fluorescence intensity of **6** is *ca.* 52-fold larger than that of **2a** in the crystalline state. The red-shifts of the longest wavelengths of the excitation and the emission maxima of **6** and **7** in the solid state are small

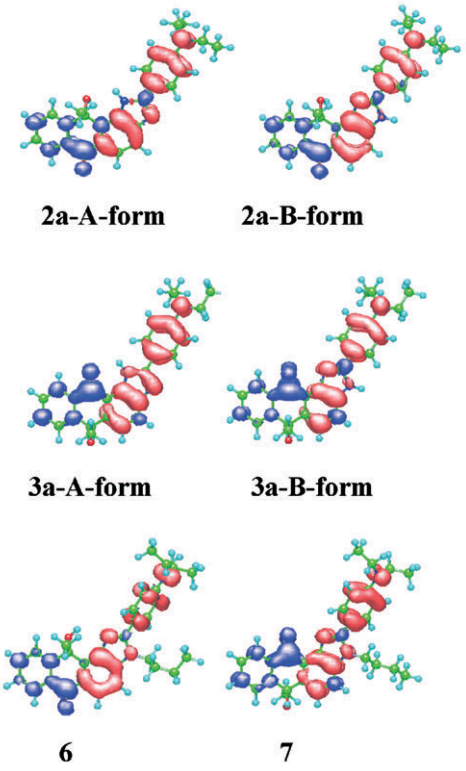

Fig. 2 Calculated electron density changes accompanying the first electronic excitation of **2a**, **3a** (A-form and B-form), **6** and **7**. The red and blue lobes signify decrease and increase in electron density accompanying the electronic transition. Their areas indicate the magnitude of the electron density change.

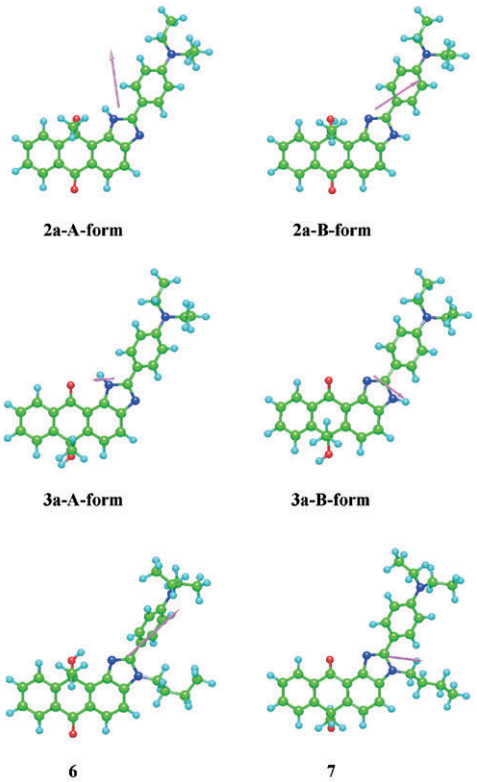

Fig. 3 The directions of dipole moments of **2a**, **3a** (A-form and B-form), **6** and **7**.

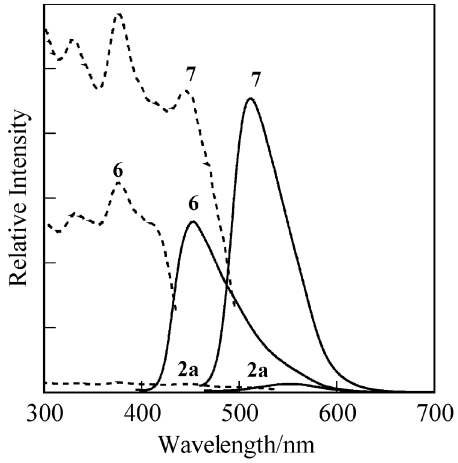

Fig. 4 Solid-state excitation (···) and emission (—) spectra of the crystals of **2a**, **6** and **7**; **2a**: $\lambda_{ex} = 520$ nm, $\lambda_{em} = 567$ nm; **6**: $\lambda_{ex} = 413$ nm, $\lambda_{em} = 457$ nm; **7**: $\lambda_{ex} = 445$ nm, $\lambda_{em} = 513$ nm.

compared to those of **6** and **7** in benzene, which is a quite different behaviour from **2a**. These results indicate that the larger the red-shift value of the absorption and the fluorescence maximum from the solution to the solid state, the greater the fluorescence quenching.

X-Ray crystal structures of the imidazoanthraquinol fluorophores

In order to investigate the effect of the crystal structure on the solid-state photophysical properties, we have performed X-ray crystallographic analysis of **2a**, **3a**, **6** and **7**. The crystal systems were a monoclinic space group $P2_1/c$ with $Z = 4$ for **2a**, an orthorhombic space group $Pna2_1$ with $Z = 4$ for **3a**, a monoclinic space group $P2_1/c$ with $Z = 4$ for **6** and a monoclinic space group $P2_1/n$ with $Z = 4$ for **7** (Table S1‡). In the crystal packing structures of **2a**, **6** and **7**, the two host enantiomers are arranged to form a centrosymmetric dimer unit in which a large dipole moment of the host molecules is counteracted. However, such arrangement is not observed in the crystal packing structure of **3a**, because of small dipole moment of **3a** in the A-form. The packing structures demonstrate that the all quinols except for **3a** are built up from a centrosymmetric dimer unit, and that the molecules are arranged in a "herringbone" fashion in **2a**, **3a** and **7** and in a "bricks in a wall" fashion in **6**, respectively.

Fig. 5(a) shows the molecular packing structure for the crystal of **2a**. The tautomeric form for the crystal of **2a** is A-form. The crystal of **2a** having the herringbone packing is built up by a centrosymmetric dimer unit which is composed of a pair of enantiomers bound cofacially by two intermolecular hydrogen bonds between the hydroxyl oxygen and imidazole nitrogen through the hydroxyl proton, which is realized on both sides of the molecules (O(1)H(1)···N(2)* angle = 168(4)°, O(1)···N(2)* distance = 2.985 (4) Å) as shown in Fig. 5(b). The phenyl group is twisted out of the plane of the heterocyclic quinol skeleton by 12.0°, which is smaller than that of the optimized geometries of **2a** (28.5° in Table 3) by MOPAC/AM1 calculations. The intramolecular hydrogen bonding formation is also observed between the imidazole amino proton and the hydroxyl oxygen in each quinol molecule (N(1)H(2)···O(1) angle = 115(2)°, N(1)···O(1) distance = 2.894(3) Å). A side view of the dimer unit and its upside view together with the non-bonded interatomic distances of less than 3.60 Å are shown in Fig. 5(c) and (d), respectively. The π-stacking between a pair of quinol enantiomers is overlapping the whole molecule from the donor unit of *p*-diethylaminophenyl moiety to the acceptor unit of imidazoanthraquinol moiety, there are 18 (= 9 × 2) short interatomic π–π contacts in the pair of enantiomers. The interplanar distance between the imidazole plates is *ca.* 3.39 Å, which suggests strong π–π interactions. No hydrogen bonding interactions and no short π–π contacts of less than 3.60 Å are observed between neighbouring units. Therefore, such strong intermolecular interactions between the enantiomers are considered to induce the large red-shift of the absorption and fluorescence maxima and an intense fluorescence quenching in the crystalline state.

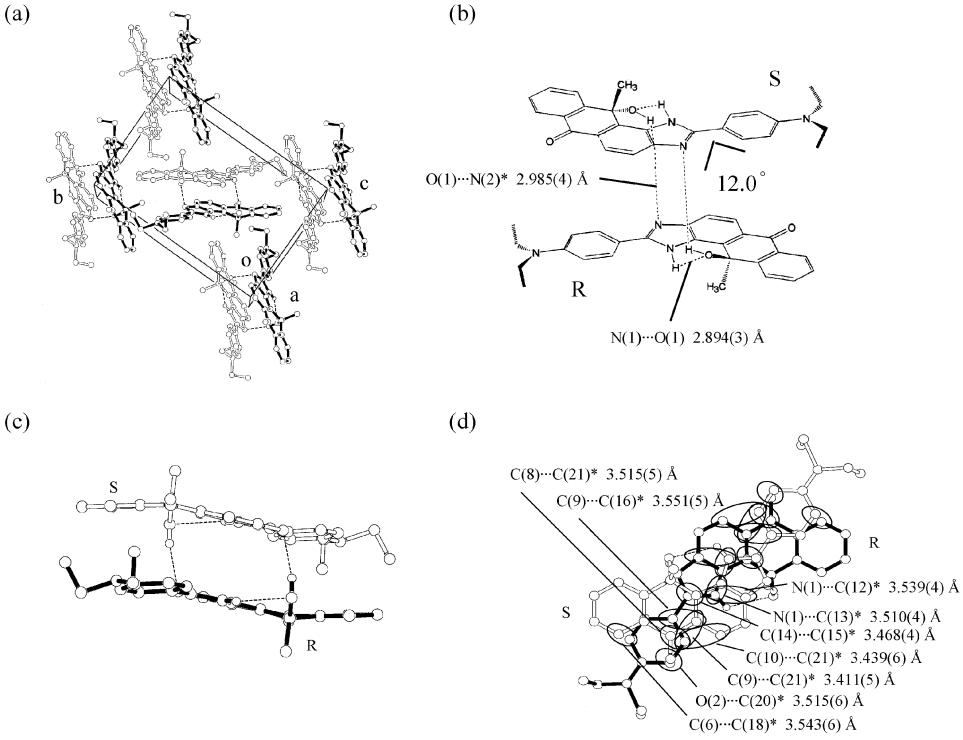

Fig. 5 Crystal packing and hydrogen bonding pattern of **2a**: (a) a stereoview of the molecular packing structure, and (b) a schematic structure, (c) a side view, and (d) a top view of the pairs of enantiomers.

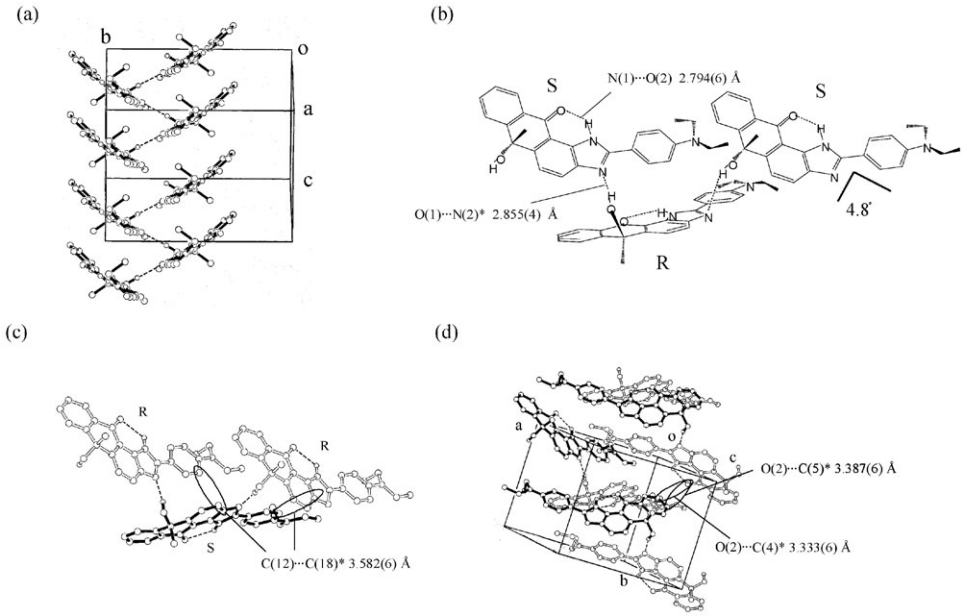

Fig. 6 Crystal packing and hydrogen bonding pattern of **3a**: (a) a stereoview of the molecular packing structure, and (b) a schematic structure, (c) intra- and intermolecular hydrogen bond between enantiomers and (d) the nearest contact between enantiomers.

Fig. 6(a) shows the molecular packing structure for the crystal of **3a**. The tautomeric form for the crystal of **3a** is the A-form. The phenyl group is twisted out of the plane of the heterocyclic quinol skeleton by 4.8° as shown in Fig. 6(b). The value of torsion angle of **3a** in the crystalline state is smaller than that of the optimized geometries of **3a** (27.8° in Table 3) by MOPAC/AM1 calculations. The intramolecular hydrogen bonding formation is observed between the imidazole amino proton and the carbonyl oxygen (N(1)H(2)···O(2) angle = 112(3)°, N(1)···O(2) distance = 2.794(6) Å). Furthermore, a one-dimensional chain is formed through the intermolecular hydrogen bonding between the hydroxyl proton and imidazole nitrogen of neighbouring enantiomers, which contributes to stabilize the crystal structure (O(1)H(1)···N(2)* angle = 158(4)°, O(1)···N(2)* distance = 2.855(4) Å). The existence of the intermolecular hydrogen bonding may raise the melting temperature: the melting point of **3a** (223–224 °C) is considerably higher than that of the structural isomer **2a** (decomposition at 180 °C). As shown in Fig. 6(c) and (d), there are three kinds of non-bonded short interatomic contacts of less than 3.60 Å within a one-dimensional chain (C(12)···C(18)* = 3.582(6) Å) and between the one-dimensional chains (O(2)···C(5)* = 3.387(6) Å and O(2)···C(4)* = 3.333(6) Å). These results suggest that non-fluorescence of **3a** in the crystalline state is attributed to the A-form being unfavourable for donor–acceptor conjugation and the large-range intermolecular hydrogen bonds forming a one-dimensional chain[16] and that non-bonded short interatomic contacts between the fluorophores would also be the factors for fluorescence quenching in the solid state.

Fig. 7(a) shows the molecular packing structure for the crystal of **6**. The crystal of **6** has stacking arrangement that avoid short contacts between the chromophores. The formation of intramolecular hydrogen bonding is observed between the hydroxyl oxygen and imidazole nitrogen through the hydroxyl proton (O(1)H(1)···N(1) angle = 145(2)°, O(1)···N(1) distance = 2.852(2) Å) (Fig. 7(b)). However, there are no intermolecular hydrogen bonding interactions and no

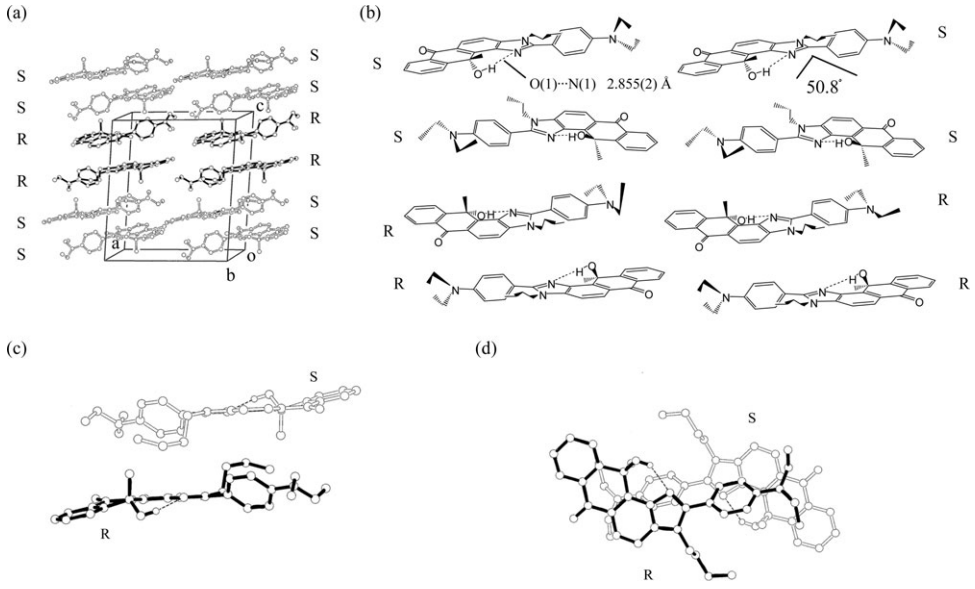

Fig. 7 Crystal packing and hydrogen bonding pattern of **6**: (a) a stereoview of the molecular packing structure, and (b) a schematic structure, (c) a side view and (d) a top view of the pairs of enantiomers.

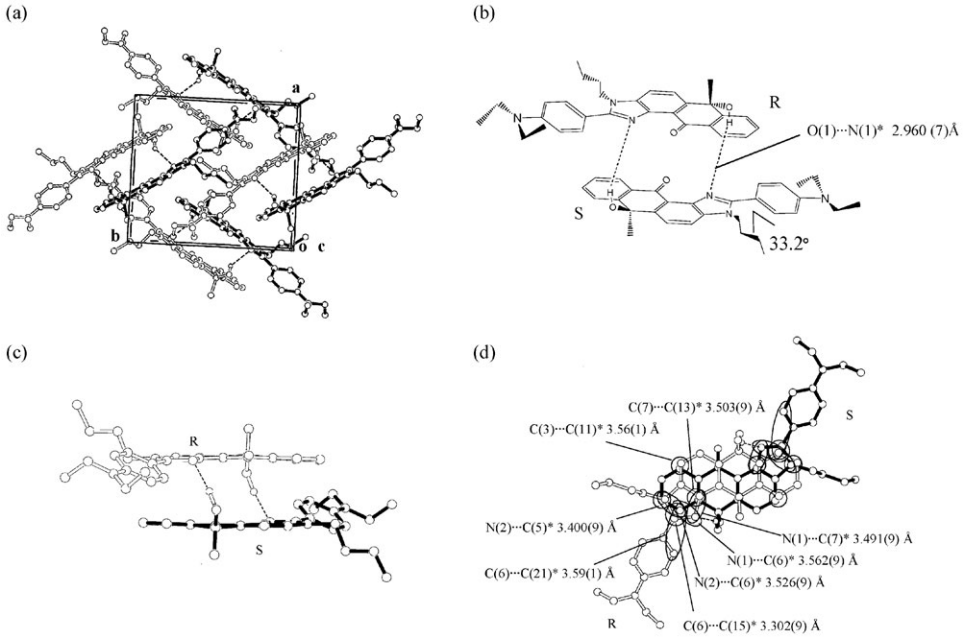

Fig. 8 Crystal packing and hydrogen bonding pattern of **7**: (a) a stereoview of the molecular packing structure, and (b) a schematic structure, (c) a side view and (d) a top view of the pairs of enantiomers.

short π–π contacts of less than 3.60 Å between the neighbouring fluorophores (Fig. 7(c) and (d)). The phenyl group is twisted out of the plane of the heterocyclic quinol skeleton by 50.8°, which is large compared to the torsion angle of **2a**. The value of the torsion angle of **6** in the crystalline state is close to that of the optimized geometries of **6** (55.4° in Table 3) by MOPAC/AM1 calculations. It is clear that the large torsion angle of **6** is attributed to the steric effect of the *N*-butyl group. Consequently, the *N*-butylation of imidazole ring of **2a** prevents the formation of intermolecular hydrogen bonding and short π–π contacts between the fluorophores in the solid state, which leads to the crystal of **6** exhibiting much stronger fluorescence with a blue-shift of the fluorescence wavelength compared to the crystal of **2a**.

On the other hand, the crystal of **7** is built up by a centrosymmetric dimer unit which is composed of a pair of quinol enantiomers bound cofacially by two intermolecular hydrogen bonds between the hydroxyl oxygen and imidazole nitrogen through the hydroxyl proton (O(1)H(1)···N(1)* angle = 173(12)°, O(1)···N(1)* distance = 2.960(7) Å), which is realized on both sides of the molecules (Fig. 8(a) and (b)). The phenyl group is twisted out of the plane of the heterocyclic-quinol skeleton by 33.2°, which is large compared to the case of **3a**. The value of torsion angle of **7** in the crystalline state is smaller than that of the optimized geometries of **7** (49.1° in Table 3) by MOPAC/AM1 calculations. As shown in Fig. 8(c) and (d), the π-stacking between a pair of enantiomers is observed between the acceptor units of imidazoanthraquinol moiety. There are 16 short interatomic π–π contacts of less than 3.6 Å in the pair of enantiomers. The interplanar distance between the imidazoanthraquinole plates is *ca.* 3.45 Å, suggesting a strong offset-like π–π stacking.[17] Considering the strong solid-emissive properties of **7**, such an offset-like π-stacking may not cause a significant fluorescence quenching. The fixation of the tautomeric form by the *N*-butylation to produce **7** having a favourable structure for a donor–acceptor conjugation system is considered the second reason for the improvement of the solid-emissive properties.

Conclusion

We have developed novel imidazoanthraquinol fluorophores that undergo tautomerism on the imidazole ring. Intense solid-state fluorescence compounds have been prepared by control of the tautomeric form by *N*-alkylation of the imidazole ring. The relationship between the photophysical properties and the chemical and crystal structures has been elucidated by means of semi-empirical MO calculations (AM1 and INDO/S) and the X-ray crystallographic analysis. The intermolecular π–π interactions and hydrogen bonding between neighbouring fluorophores are found to influence the solid-state photophysical properties, such as absorption and fluorescence wavelengths and solid-state fluorescence intensity. The effectiveness of the control of the tautomeric form and the crystal structure, which is important for both the basic science and the development of new solid-emissive materials, has been shown.

We have further found that the fluorophore **2** undergo a dramatic fluorescence enhancement behaviour upon enclathration of various kinds of organic solvent molecules. The details of the solid-state fluorescence enhancement behaviour will be reported in this series.

Experimental

Melting points were measured with a Yanaco micro melting point apparatus MP-500D. IR spectra were recorded on a JASCO FT/IR-5300 spectrophotometer for samples in KBr pellet form. Absorption spectra were observed with a JASCO U-best30 spectrophotometer and fluorescence spectra were measured with a JASCO FP-777 spectrophotometer. Single-crystal X-ray diffraction was performed on Rigaku AFC7S diffractometer. Absorption spectra were measured with U-best-30 spectrophotometer. For the measurement of the solid-state fluorescence excitation and emission spectra of the crystals, a JASCO FP-777 spectrometer equipped with a JASCO FP-1060 attachment was used. The fluorescence quantum yields (Φ) were determined using 9,10-diphenylanthracene (Φ = 0.67, λ_{ex} = 357 nm)[18] in benzene as the standard. Elemental analyses were recorded on a Perkin Elmer 2400 II CHN analyzer. ^{1}H NMR spectra were recorded on a JNM-LA-400 (400 MHz) FT NMR spectrometer with tetramethylsilane (TMS) as an internal standard. Column chromatography was performed on silica gel (KANTO CHEMICAL, 60N, spherical, neutral) or alumina (WAKO, about 300 mesh). Semi-empirical molecular orbital (MO) calculations were

performed on FUJITSU FMV-ME4/657 by using the WinMOPAC Ver. 3 package (Fujitsu, Chiba, Japan).

Synthesis of 2-[(4-diethylamino)phenyl]imidazo [5,4-*a*]anthraquinone (1)

To a solution of *p*-diethylaminobenzaldehyde (2.23 g, 12.6 mmol) and $Cu(OCOCH_3)_2$ (4.58 g, 25.2 mmol) in acetic acid (100 ml) was add dropwise a solution of 1,2-diaminoanthraquinone (3.00 g, 12.6 mmol) in acetic acid (100 ml) with stirring at 90 °C. After further stirring for 2 h, the solvent was removed and the black residue was extracted with $CHCl_3$. The organic extract was washed with water, dried and concentrated. The deep red residue was chromatographed on silica gel (CH_2Cl_2 : ethyl acetate = 3 : 1 as eluent) to give **1** (3.83 g, yield 77%); m.p. 228–229 °C; IR(KBr)/cm^{-1} 3439 (NH), 1606 (C═O); ^1H NMR ($CDCl_3$/TMS) δ = 1.24 (6H, t), 3.46 (4H, q), 6.77 (2H, d, J = 9.0 Hz), 7.77–7.80 (2H, m), 7.98 (2H, d, J = 9.0 Hz), 8.01 (1H, d, J = 8.3 Hz), 8.19 (1H, d, J = 8.3 Hz), 8.25–8.28 (1H, m), 8.32-8.34 (1H, m), 11.08 (1H, br) (Found: C, 76.06; H, 5.32; N, 10.33. $C_{25}H_{21}N_3O_2$ requires C, 75.93; H, 5.37; N, 10.63%).

Synthesis of isomeric quinols 2a–2b and 3a–3c by the reaction of 1 with organolithium or Grignard reagents

General procedure. To a THF solution (200 ml) of **1** under an Ar atmosphere was added ethereal solution of organolithium (RLi: MeLi, BuLi and PhLi) or MeMgBr at −108 °C over 15 min. During the course of addition, the red solution turned to a reddish brown solution. After stirring for 15 min at room temperature, the reaction was quenched with saturated NH_4Cl solution. The solvent was evaporated and the residue was extracted with CH_2Cl_2. The organic extract was washed with water. The CH_2Cl_2 extract was evaporated and the residue was chromatographed on alumina (CH_2Cl_2 as eluent). The column chromatography gave **1** and a mixture of **2** and **3**. The mixture was chromatographed on silica gel (CH_2Cl_2 : AcOEt = 3 : 1 as eluent) to give **2** as an orange powder, **3** as a brown-red powder. The yields of **2** and **3** and the recovery of **1** are shown in Table 1.

2-[(4-Diethylamino)phenyl]-11-hydroxy-11-methylimidazo [5,4-*a*]-anthracen-6(11*H*)-one (2a)

178–180 °C (decomposition); IR (KBr)/cm^{-1} 3445 (NH), 3223 (OH), 1647(C═O); ^1H NMR ($CDCl_3$, TMS) δ = 1.09 (6H, t), 1.79 (3H, q), 3.38 (4H, q), 6.59 (1H, s), 6.74 (2H, d, J = 9.0 Hz), 7.38–7.45 (1H, m), 7.47 (1H, d, J = 8.5 Hz), 7.60–7.64 (1H, m), 7.94 (1H, d, J = 8.5 Hz), 7.95 (1H, d, J = 0.73 Hz), 7.99 (2H, d, J = 9.0 Hz), 8.09 (1H, d, J = 0.73 Hz) (Found: C, 75.89; H, 6.29; N, 10.31. $C_{26}H_{25}N_3O_2$ requires C, 75.89; H, 6.12; N, 10.21%).

2-[(4-Diethylamino)phenyl]-6-hydroxy-6-methylimidazo [5,4-*a*]anthracen-11(6*H*)-one (3a)

Mp 223–224 °C; IR (KBr)/cm^{-1} 3435 (NH), 3207 (OH), 1647 (C═O); ^1H NMR (CD_3COCD_3, TMS) δ = 1.08 (6H, t), 1.60 (3H, s), 3.38 (4H, q), 4.96 (1H, s), 6.73 (2H, d, J = 9.0 Hz), 7.41 (1H, td, J = 1.2 and 6.6 Hz), 7.63 (1H, td, J = 1.2 and 6.6 Hz), 7.69–7.71 (1H, m), 7.80–7.82 (1H, m), 7.95–7.97 (1H, m), 8.08 (2H, d, J = 9.0 Hz), 8.09–8.11 (1H, m), 11.46 (1H, Br). (Found: C, 76.07; H, 6.20; N, 10.17. $C_{26}H_{25}N_3O_2$ requires: C, 75.89; H, 6.12; N, 10.21%).

2-[(4-Diethylamino)phenyl]-11-butyl-11-hydroxyimidazo [5,4-*a*]-anthracen-6(11*H*)-one (2b)

166–167 °C (decomposition); IR (KBr)/cm^{-1} 3435 (NH), 1641 (C═O); ^1H NMR(DMSO, TMS) δ = 0.51 (3H, t), 0.60 (2H, m), 0.88 (2H, m), 1.15 (6H, t), 2.12 (2H, m), 3.44 (4H, q), 6.67 (1H, s), 6.84 (2H, d, J = 8.5 Hz), 7.55 (1H, t, J = 7.3 Hz), 7.59–7.61 (1H, m), 7.77 (1H, t, J = 7.3 Hz), 7.96 (2H, d, J = 8.5 Hz), 8.04 (1H, d, J = 8.8 Hz), 8.13–8.15 (1H, m), 8.20 (1H, d, J = 8.8 Hz), 11.95 (1H, br). (Found: C, 76.59; H, 6.75; N, 9.11. $C_{29}H_{31}N_3O_2$ requires: C, 76.79; H, 6.89; N, 9.26%).

2-[(4-Diethylamino)phenyl]-6-butyl-6-hydroxyimidazo [5,4-*a*]anthracen-11(6*H*)-one (3b)

Mp 185–187 °C; IR (KBr)/cm^{-1} 3445 (NH), 1647 (C═O); ^1H NMR (CD_3COCH_3, TMS) δ = 0.58 (3H, t), 0.64 (2H, m), 1.00 (2H, m), 1.21 (6H, t), 2.11 (2H, m), 3.49 (4H, q), 5.18 (1H, s), 6.83 (2H, d, J = 8.5 Hz), 7.52 (1H, t, J = 7.8 Hz), 7.74 (1H, t, J = 7.8 Hz), 7.76–7.79 (1H, m), 7.89–7.92 (1H, m), 8.02–8.04 (1H, m), 8.17 (2H, d, J = 8.5 Hz), 8.20–8.22 (1H, m), 11.55 (1H, br). (Found: C, 76.51; H, 6.85; N, 9.21. $C_{29}H_{31}N_3O_2$ requires: C, 76.79; H, 6.89; N, 9.26%).

Synthesis of 2-[(4-diethylamino)phenyl]-6-hydroxy-6-phenyl-imidazo[5,4-*a*]-anthracen-11(6*H*)-one (3c)

Mp 226–230 °C; IR (KBr)/cm^{-1} 3439 (NH), 1643 (C═O); ^1H NMR ($CDCl_3$, TMS) δ = 1.15 (6H, t), 3.44 (4H, q), 6.77 (2H, d, J = 8.5 Hz), 6.95 (1H, s), 7.08–7.11 (1H, m), 7.19–7.23 (2H, m), 7.30–7.32 (2H, m), 7.36 (1H, d, J = 8.3 Hz), 7.52 (1H, t, J = 7.8 Hz), 7.63 (1H, t, J = 7.8 Hz), 7.64 (1H, d, J = 7.8 Hz), 7.82 (1H, d, J = 8.3 Hz), 8.18 (2H, d, J = 8.5 Hz), 8.22 (1H, d, J = 7.8 Hz), 12.43 (1H, Br). (Found: C, 76.47; H, 5.66; N, 8.57. $C_{31}H_{27}N_3O_2$ requires C, 78.62; H, 5.75; N, 8.87%).

Synthesis of 3-butyl-2-[(4-diethylamino)phenyl]-3*H*-anthra [1,2-*a*]imidazole-6,11-dione (5)

To a solution of 1,2-diaminoanthraquinone (5.0 g, 21 mmol), *N*-methyl pyrrolidone (80 ml), and sodium carbonate (25 ml) was added dropwise a solution of butyl iodide (11.58 g, 63 mmol) in *N*-methyl pyrrolidone (30 ml) with stirring at 90 °C. After further stirring for 3 h at the same temperature, to the reaction mixture was added water, then a black-purple precipitate was obtained, which was separated by filtration and recrystallized from pyridine–water to give 1-amino-2-butyl-amino-anthraquinone (**4**) (4.12 g, 66%).

To a solution of *p*-diethylaminobenzaldehyde (2.23 g, 12.6 mmol) and $Cu(OCOCH_3)_2$ (4.58 g, 25.2 mmol) in acetic acid (100 ml) was added dropwise the above compound (**4**) (3.71 g, 12.6 mmol) in acetic acid solution (100 ml) with stirring at 90 °C. After further stirring for 2 h at the same temperature, the solvent was removed and the red-brown residue was extracted with CH_2Cl_2. The organic extract was washed with water, dried and concentrated. The red residue was chromatographed on silica gel (CH_2Cl_2 : ethyl acetate = 3 : 1 as eluent) to give **5** (4.38 g, yield 77%): mp 145–146 °C; IR (KBr)/cm^{-1} 1608 (C═O); ^1H NMR (DMSO/TMS) δ = 0.82 (3H, t), 1.15 (6H, t), 1.20–1.26 (2H, m), 1.70–1.74 (2H, m), 3.44 (4H, q), 4.40 (2H, t), 6.86 (2H, d, J = 9.0 Hz), 7.71 (2H, d, J = 8.8 Hz), 7.85–7.92 (2H, m), 8.07–8.18 (4H, m). (Found: C, 76.96; H, 6.62; N, 9.33. $C_{29}H_{29}N_3O_2$ requires: C, 77.13; H, 6.47; N, 9.31%).

Synthesis of isomeric quinols 6 and 7 by the reaction of 5 with methyllithium

To a THF solution (400 ml) of **5** under an Ar atmosphere was added 1.0 equivalent of an ethereal solution of methyllithium at −108 °C over 30 min. During the course of addition, the red

solution turned to a reddish brown suspension. After stirring for 30 min, the reaction was quenched with saturated aqueous NH_4Cl. The solvent was evaporated and the residue was extracted with CH_2Cl_2. The organic extract was washed with water. The CH_2Cl_2 solvent was evaporated and the residue was chromatographed on alumina (CH_2Cl_2 as eluent). The column chromatography gave **5** and a mixture of **6** and **7**. The mixture was further chromatographed on silica gel (CH_2Cl_2 : ethyl acetate = 3 : 1 as eluent) to give **6** (30%) as a yellowish green powder, **7** (43%) as a yellow powder.

3-Butyl-2-[(4-diethylamino)phenyl)]-11-hydroxy-11-methyl-1*H*, 11*H*-anthra[1,2-*a*]imidazol-6-one (6)

Mp 167–168 °C; IR (KBr)/cm^{-1} 3061 (OH), 1608 (C=O); ^{1}H NMR (DMSO/TMS) δ = 0.83 (3H, t), 1.15 (6H, t), 1.23–1.29, (2H, m), 1.74–1.77 (2H, m), 1.89 (3H, s), 3.43 (4H, q), 4.39(2H, t), 6.41(1H, s), 6.85 (2H, d, J = 9.0 Hz), 7.54 (1H, t, J = 7.1 Hz), 7.68 (2H, d, J = 9.0 Hz), 7.77 (1H, t, J = 7.1 Hz), 7.78 (1H, d, J = 8.5 Hz), 7.98 (1H, d, J = 7.1 Hz), 8.05 (1H, d, J = 8.5 Hz), 8.13–8.15 (1H, m). (Found: C, 76.93; H, 7.19; N, 8.99. $C_{30}H_{33}N_3O_2$ requires: C, 77.06; H, 7.11; N, 8.99%).

3-Butyl-2-[(4-diethylamino)phenyl)]-6-hydroxy-6-methyl-3*H*, 6*H*-anthra[1,2-*a*]imidazol-11-one (7)

Mp 228–230 °C; IR (KBr)/cm^{-1} 3443 (OH), 1607 (C=O); ^{1}HNMR (DMSO/TMS) δ = 0.81 (3H, t) 1.15 (6H, t), 1.21 (2H, m), 1.58 (3H, s), 1.71 (2H, m), 3.43 (4H, q), 4.35 (2H, t), 6.17 (1H, s), 6.83 (2H, d, J = 9.0 Hz), 7.48–7.51 (1H, m), 7.64 (2H, d, J = 9.0 Hz), 7.67-7.71 (1H, m), 7.82 (1H, d, J = 8.5 Hz), 7.94 (1H, d, J = 8.5 Hz), 7.95–7.97 (1H, m), 8.03–8.05 (1H, m). (Found: C, 76.80; H, 7.17; N, 8.82. $C_{30}H_{33}N_3O_2$ requires: C, 77.06; H, 7.11; N, 8.99%).

Computational methods

All calculations were performed on FUJITSU FMV-ME4/657. The semi-empirical calculations were carried out with the WinMOPAC Ver. 3 package (Fujitsu, Chiba, Japan). Geometry calculations in the ground state were carried out using the AM1 method.[10] All geometries were completely optimized (keyword PRECISE) by the eigenvector following routine (keyword EF). Experimental absorption spectra of the seven quinol derivatives were studied with the semi-empirical method INDO/S (intermediate neglect of differential overlap/spectroscopic).[9] All INDO/S calculations were performed using single excitation full SCF/CI (self-consistent field/configuration interaction), which includes the configuration with one electron excited from any occupied orbital to any unoccupied orbital, 225 configurations were considered for the configuration interaction [keyword CI (15 15)].

X-ray crystallographic studies §

The reflection data were collected at 23 ± 1 °C on a Rigaku AFC7S four-circle diffractometer by 2θ-ω scan technique, and using graphite-monochromated Mo-Kα (λ = 0.710 69 Å) radiation at 50 kV and 30 mA. In all case, the data were corrected for Lorentz and polarization effects. A correction for secondary extinction was applied. Crystal data, data collection and refinement parameters are summarized in Table S1. The reflection intensities were monitored by three standard reflections for every 150 reflections. An empirical absorption correction based on azimuthal scans of several reflections was applied. All calculations were performed using the teXsan[19] crystallographic software package of Molecular Structure Corporation.

Crystal structure determination of compound 2a

Crystals of **2a** were recrystallized from dichloromethane–n-hexane as air stable orange prisms. The one selected had approximate dimensions 0.45 × 0.25 × 0.45 mm. The transmission factors ranged from 0.97 to 1.00. The crystal structure was solved by direct methods using SIR 92.[20] The structures were expanded using Fourier techniques.[21] The non-hydrogen atoms were refined anisotropically. Some hydrogen atoms were refined isotropically, the rest were fixed geometrically and not refined.

Crystal data. $C_{26}H_{25}N_3O_2$, M = 411.50, monoclinic, a = 11.111(2), b = 16.954(2), c = 12.318(2) Å, β = 113.97(1)°, U = 2120.3(5) Å^3, T = 296.2 K, space group $P2_1/c$ (no. 14), Z = 4, μ(Mo-K$_a$) = 0.8 cm^{-1}, 3936 reflections measured, 3735 unique (R_{int} = 0.020) which were used in all calculations. The final R indices [$I > 2\sigma(I)$], $R1$ = 0.0623, $wR(F^2)$ = 0.1457.

Crystal structure determination of compound 3a

Crystals of **3a** were recrystallized from dichloromethane–n-hexane as air stable orange-brown prisms. The one selected had approximate dimensions 0.30 × 0.45 × 0.25 mm. The transmission factors ranged from 0.98 to 1.00. The crystal structure was solved by direct methods using SIR 92.[20] The structures were expanded using Fourier techniques.[21] The non-hydrogen atoms were refined anisotropically. Some hydrogen atoms were refined isotropically, the rest were fixed geometrically and not refined.

Crystal data. $C_{26}H_{25}N_3O_2$, M = 411.50, orthorhombic, a = 13.405(6), b = 10.911(2), c = 14.405(3) Å, U = 2106(1) Å^3, T = 296.2 K, space group $Pna2_1$ (no.33), Z = 4, μ(Mo-K_a) = 0.8 cm^{-1}, 2758 reflections measured, 2516 unique (R_{int} = 0.000) which were used in all calculations. The final R indices [$I > 2\sigma(I)$], $R1$ = 0.0424, $wR(F^2)$ = 0.0987.

Crystal structure determination of compound 6

Crystals of **6** were recrystallized from ethanol as air stable yellowish green prisms. The one selected had approximate dimensions 0.60 × 0.20 × 0.40 mm. The transmission factors ranged from 0.92 to 0.99. The crystal structure was solved by direct methods using SIR 92.[20] The structures were expanded using Fourier techniques.[21] The non-hydrogen atoms were refined anisotropically. Some hydrogen atoms were refined isotropically, the rest were fixed geometrically and not refined.

Crystal data. $C_{30}H_{33}N_3O_2$, M = 467.61, monoclinic, a = 16.130(3), b = 8.793(3), c = 18.260(3) Å, β = 96.12(1)°, U = 2575.1(9) Å^3, T = 296.2 K, space group $P2_1/c$ (no. 14), Z = 4, μ(Mo-K$_a$) = 0.8 cm^{-1}, 4697 reflections measured, 4696 unique (R_{int} = 0.017) which were used in all calculations. The final R indices [$I > 2\sigma(I)$], $R1$ = 0.0439, $wR(F^2)$ = 0.1093.

Crystal structure determination of compound 7

Crystals of **7** were recrystallized from ethanol as air stable yellow prisms. The one selected had approximate dimensions 0.20 × 0.10 × 0.20 mm. The transmission factors ranged from 0.93 to 1.00. The crystal structure was solved by direct methods using SIR 92.[20] The structures were expanded using Fourier techniques.[21] The non-hydrogen atoms were refined anisotropically. Some hydrogen atoms were refined isotropically, the rest were fixed geometrically and not refined.

§ CCDC reference numbers 236773–236776. See http://www.rsc.org/suppdata/nj/b4/b410311d/ for crystallographic data in .cif or other electronic format.

Crystal data. $C_{30}H_{33}N_3O_2$, $M = 467.61$, monoclinic, $a = 12.007(3)$, $b = 13.152(4)$, $c = 16.196(5)$ Å, $\beta = 102.99(2)^\circ$, $U = 2492(1)$ Å^3, $T = 296.2$ K, space group $P2_1/n$ (no.14), $Z = 4$, μ(Mo-K$_a$) = 0.8 cm^{-1}, 4766 reflections measured, 4390 unique ($R_{int} = 0.095$) which were used in all calculations. The final R indices [$I > 2\sigma(I)$], $R1$=0.0763, $wR(F^2) = 0.1490$.

Acknowledgements

This work was partially supported by Regional Science Promotion (RSP) program by the Ministry of Education, Culture, Sports, Science and Technology (MEXT), Japan. Y.O. was supported by a research fellowships from the Japan Society for the Promotion of Science (JSPS) for young scientists.

References

1 (*a*) C. W. Tang and S. A. VansSlyke, *Appl. Phys. Lett*., 1987, **51**, 913; (*b*) C. W. Tang, S. A. VansSlyke and C. H. Chen, *J. Appl. Phys*., 1989, **65**, 3610; (*c*) J. Schi and C. W. Tang, *Appl. Phys. Lett*., 1997, **70**, 1665; (*d*) K. Köller, *Appl. Fluorescence Technol*., 1989, **1**, 1; (*e*) A. Kraft, A. C. Grimsdale and A. B. Holmes, *Angew. Chem. Int. Ed*., 1998, **37**, 402; (*f*) R. H. Friend, R. W. Gymer, A. B. Holmes, J. H. Burroughes, R. N. Marks, C. Taliani, D. D. C. Bradley, D. A. DosSantos, J. L. Brédas, M. LÖgdlund and W. R. Salaneck, *Nature*, 1999, **397**, 121; (*g*) U. Mitschke and P. Bäuerle, *J. Mater. Chem*., 2000, **10**, 1471; (*h*) K. Hirano, S. Minakata and M. Komatsu, *Chem. Lett*., 2001, 8; (*i*) K. Hirano, Y. Oderaotoshi, S. Minakata and M. Komatsu, *Chem. Lett*., 2001, 1262.

2 H.-J. Knölker, R. Boese and R. Hitzemann, *Chem. Ber*., 1990, **123**, 327.

3 (*a*) K. Shirai, A. Yanagizawa, H. Takahashi, K. Fukunishi and M. Matsuoka, *Dye Pigm*., 1998, **39**, 49–68; (*b*) J. H. Kim, S. R. Shin, M. Matsuoka and K. Fukunishi, *Dye Pigm*., 1998, **39**, 341–357.

4 (*a*) K. Yoshida, Y. Ooyama, H. Miyazaki and S. Watanabe, *J. Chem. Soc., Perkin Trans. 2*, 2002, 700–707; (*b*) K. Yoshida, Y. Ooyama, S. Tanikawa and S. Watanabe, *J. Chem. Soc., Perkin Trans. 2*, 2002, 708–714.

5 C. J. Tonzola, M. M. Alam, W. K. Kaminsky and S. A. Jenekhe, *J. Am. Chem. Soc*., 2003, **125**, 13548.

6 E. Horiguchi, S. Matsumoto, K. Funabiki and M. Matui, *Chem. Lett*., 2004, **170**.

7 K. Yoshida, J. Yamazaki, Y. Tagashira, H. Miyazaki and S. Watanabe, *Chem. Lett*., 1996, 9.

8 K. Yoshida, T. Tachikawa, J. Yamasaki, S. Watanabe and S. Tokita, *Chem. Lett*., 1996, 1027.

9 (*a*) J. E. Ridley and M. C. Zerner, *Theor. Chim. Acta*, 1973, **32**, 111; (*b*) J. E. Ridley and M. C. Zerner, *Theor. Chim. Acta*, 1976, **42**, 223; (*c*) A. D. Bacon and M. C. Zerner, *Theor. Chim. Acta*, 1979, **53**, 21.

10 M. J. S. Dewar, E. G. Zoebisch, E. F. Healy and J. J. Stewart, *J. Am. Chem. Soc*., 1985, **107**, 389.

11 M. Adachi, Y. Murata and S. Nakamura, *J. Org. Chem*., 1993, **58**, 5238.

12 W. M. F. Fabian, S. Schuppler and O. S. Wolfbesis, *J. Chem. Soc., Perkin Trans. 2*, 1996, 853.

13 (*a*) J. Aihara, G. Kushibiki and Y. Matsunaga, *Bull. Chem. Soc. Jpn*., 1973, **46**, 3584; (*b*) J. Aihara, *Bull. Chem. Soc. Jpn*., 1974, **47**, 2063.

14 G. R. Desiraju, I. C. Paul and D. Y. Curtin, *J. Am. Chem. Soc*., 1977, **99**, 1594.

15 M. Tanaka, H. Hayashi, S. Matsumoto, S. Kashino and K. Mogi, *Bull. Chem. Soc. Jpn*., 1997, **70**, 329.

16 K. Yoshida, K. Uwada, H. Kumaoka, L. Bu and S. Watanabe, *Chem. Lett*., 2001, 808.

17 M. Cotrait, P. Marsau, L. Kessab, S. Grelier, A. Nourmamode and A. Castellan, *Aust. J. Chem*., 1994, **47**, 423.

18 C. A. Heller, R. A. Henry, B. A. Mclaughlin and D. E. Bills, *J. Chem. Eng. Data*, 1974, **19**, 214.

19 teXsan: Crystal Structure Analysis Package, Molecular Structure Corporation, The Woodlands, TX, 1985 and 1992.

20 A. Altomare, M. C. Burla, M. Camalli, M. Cascarano, C. Giacovazzo, A. Guagliardi and G. Polidori, *J. Appl. Cryst*., 1994, **27**, 435.

21 DIRDIF94. P. T. Beurskens, G. Admiraal, G. Beurskens, W. P. Bosman, R. de Gelder, R. Israel and J. M. M. Smits, The DIRIF94 program system, Technical Report of the Crystallography Laboratory, University of Nijmegen, The Netherlands, 1994.